Electronic Supplementary Material (ESI) for Chemical Communications.
This journal is © The Royal Society of Chemistry 2020

Supporting information for

Near-IR Absorbing *J*-Aggregates of a Phenanthrene-Fused BODIPY as a Highly Efficient Photothermal Nanoagent

Xing Guo,[†] Mao Li,[†] Hao Wu,[†] Wanle Sheng,[†] Yuanmei Feng,[†] Changjiang Yu,[†] Lijuan Jiao*,[†] and Erhong Hao*,[†]

[†]Laboratory of Functional Molecular Solids, Ministry of Education; School of Chemistry and Materials Science, Anhui Normal University, Wuhu, 241002, China

*E-mail: jiao421@ahnu.edu.cn; haoehong@ahnu.edu.cn

Contents

1. General information

Reagents and solvents were used as received from commercial suppliers unless noted otherwise. All reactions were performed in oven-dried or flame-dried glassware unless stated otherwise and were monitored by TLC using 0.25 mm silica gel plates with UV indicator (60F-254). ^{1}H and ^{13}C NMR spectra were recorded on a 300 or 500 MHz NMR spectrometer at room temperature. Chemical shifts (δ) are given in ppm relative to $CDCl_3$ (7.26 ppm for ^{1}H and 77 ppm for ^{13}C) or to internal TMS. High-resolution mass spectra (HRMS) or mass spectra (MS) were obtained using APCI in positive mode. Transition electron microscopic (TEM) images were obtained using a Hitachi HT7700 instrument.

UV-visible absorption and fluorescence emission spectra were recorded on commercial spectrophotometers (Shimadzu UV-2450 and Edinburgh FS5 spectrometers, 190-900 nm scan range) at room temperature (10 mm quartz cuvette). Relative fluorescence quantum efficiencies of BODIPY derivatives were obtained by comparing the areas under the corrected emission spectrum of the test sample in various solvents with Cresly Violet perchlorate (Φ_{FL} = 0.54 in methanol)[1] and 1,7-diphenyl-3,5-di(4-methoxyphenyl) -azadipyrromethene (Φ_{FL} = 0.36 in chloroform).[2] Non-degassed, spectroscopic grade solvents and a 10 mm quartz cuvette were used. Dilute solutions (0.01<A<0.05) were used to minimize the reabsorption effects. Quantum yields were determined using the following equation:

$$\Phi_X = \Phi_S (I_X/I_S) (A_S/A_X) (n_X/n_S)^3 \quad \text{eq S1}$$

Where Φ_S stands for the reported quantum yield of the standard, I stands for the integrated emission spectra, A stands for the absorbance at the excitation wavelength and *n* stands for the refractive index of the solvent being used. X subscript stands for the test sample, and S subscript stands for the standard.

2. Molecular Dynamics Simulations

We have performed the molecular dynamics simulations to determine the interactions between **pf-BDP** molecules through the software Materials Studio 7.0. The DMol^3 modules[4] were used to obtain the optimized geometries and ESP charges of **pf-BDP** molecules by the functions of generalized gradient approximation (GGA) and Perdew−Burke−Ernzerhof (PBE), with the basis set as DNP. The geometry optimized **pf-BDP** molecules were used Polymorph modules to predict crystal structure. We chose Dreiding forcefield[5] and ultra-fine quality. The energy optimization of **pf-BDP** structure through Monte Carlo Simulated annealing method and eventually exhibited 10796 kinds of possible arrangements and combination forms in three-dimensional space. Then we listed these arrangements in order from lowest to highest according to the total energy to filter possible crystal structure which has energy optimization lowest.

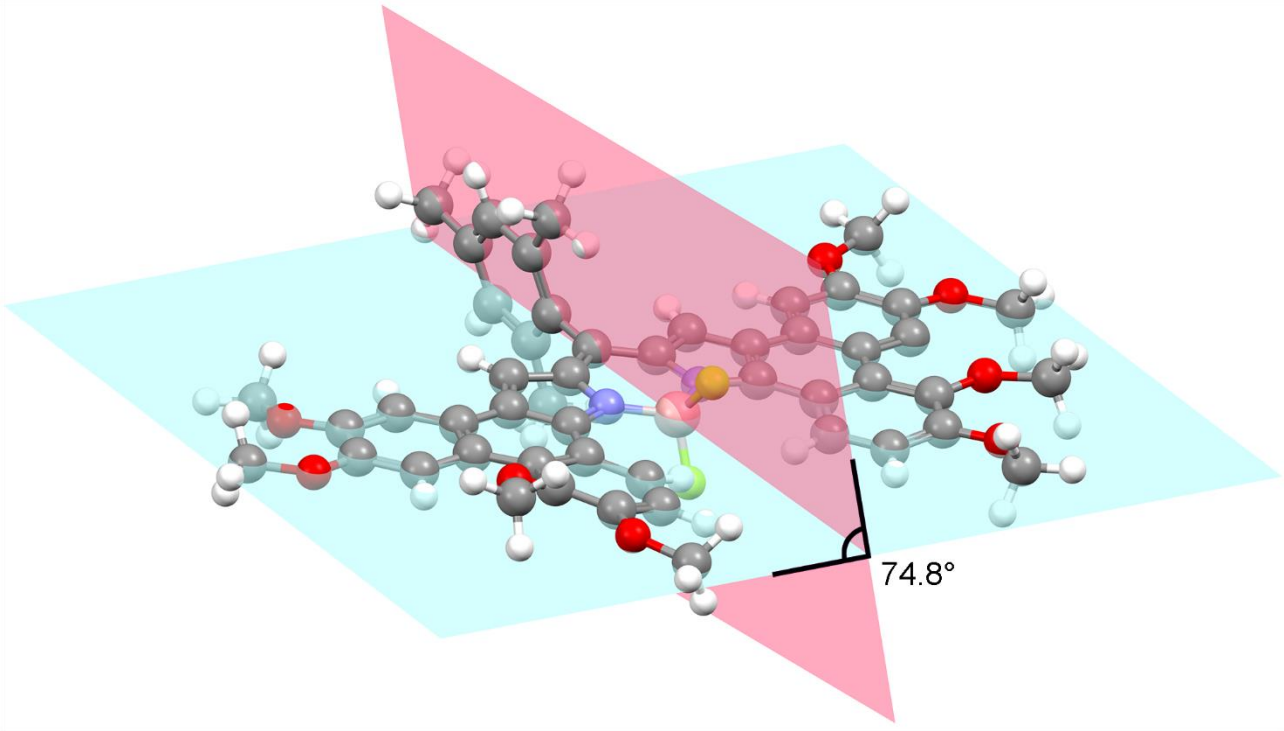

Figure S1. Molecular structure of **pf-BDP** by molecular dynamics simulation. The phenanthrene-fused dipyrrin core is essentially planar and the *meso*-mesitylene group is almost perpendiculally to the extended dipyrrin core with a dihedral angle of 74.8°.

3. Synthesis and characterization

Compound BDP were synthesized by following the procedures according to literature.[6-7]

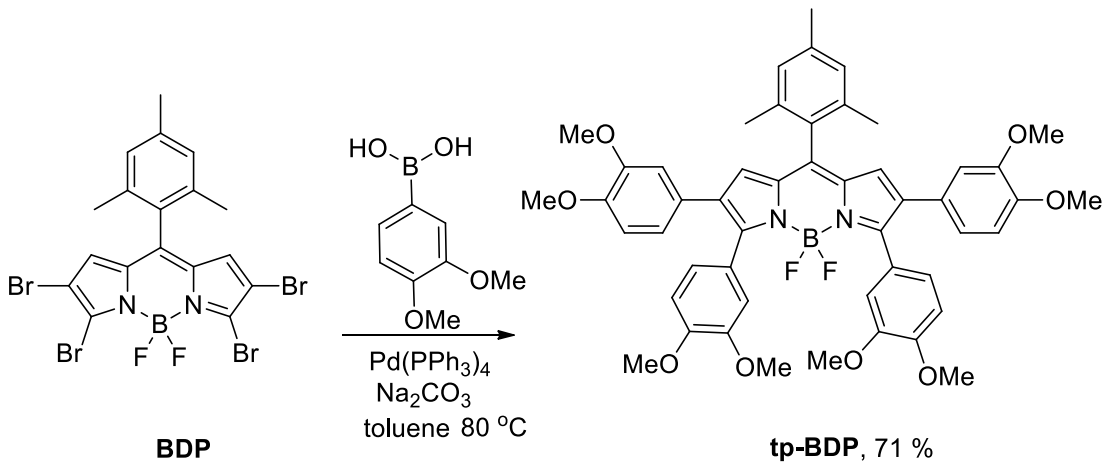

BDP **tp-BDP**, 71 %

tp-BDP: A Schelenk tube charged with **BDP** (124 mg, 0.20 mmol), 3,4-dimethoxyphenylboronic acid (182 mg, 1.00 mmol), $Pd(PPh_3)_4$ (23.1 mg, 0.02 mmol) and Na_2CO_3 (1 mol/L) were evacuated and backfilled with argon for three times. After degassed and dried toluene (5 mL) was added, the tube was heated at 80 °C for 24

h. After being cooled to room temperature, the green reaction mixture was diluted with dichloromethane (50 mL), and then washed with water (50 mL) for three times dried over anhydrous Na_2SO_4. Upon removal of solvents in vacuo, the residual was purified by silica gel column chromatography (PE/EA, 4/1, v/v) to afford compound **tp-BDP** (120 mg, 71%) as dark green solid. ^{1}H NMR (300 MHz, $CDCl_3$) δ 7.15 - 7.10 (m, 4H), 7.03 (s, 2H), 6.81 (d, J = 8.2 Hz, 2H), 6.68 - 6.62 (m, 6H), 6.46 (d, J = 1.8 Hz, 2H), 3.88 (s, 6H), 3.82 (s, 6H), 3.71 (s, 6H), 3.56 (s, 6H), 2.40 (s, 3H), 2.30 (s, 6H). ^{13}C NMR (75 MHz, $CDCl_3$) δ 155.7, 149.7, 148.3, 148.0, 138.5, 136.9, 134.7, 134.2, 130.5, 128.2, 126.8, 125.9, 124.4, 123.9, 120.8, 113.9, 111.9, 111.8, 110.9, 110.8, 110.4, 55.8, 55.7, 55.6, 21.2, 20.4. HRMS (APCI) calcd. for $C_{50}H_{49}BF_2N_2O_8$ $[M + H]^+$ 855.3623, found 855.3620.

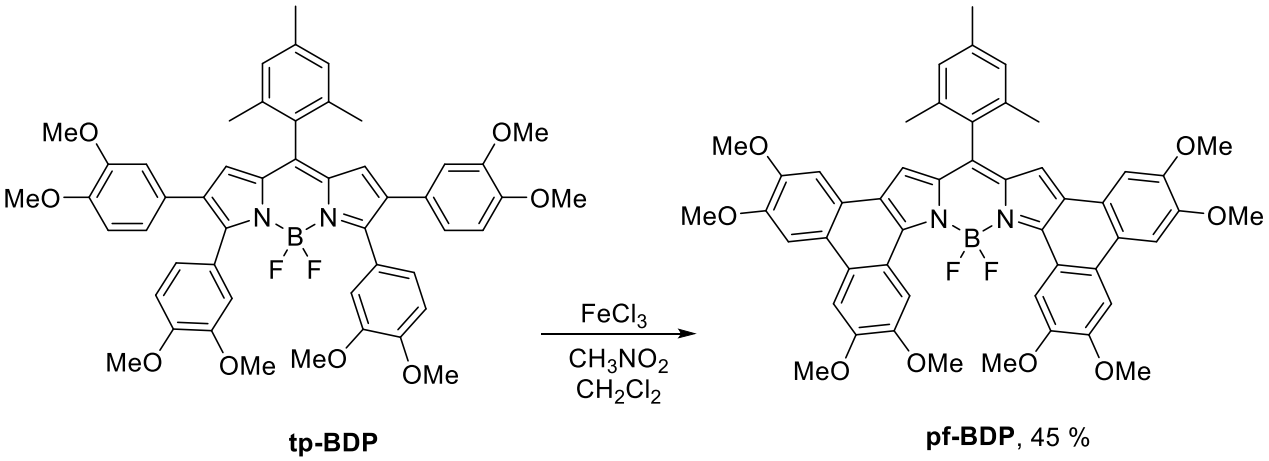

tp-BDP **pf-BDP**, 45 %

pf-BDP: To a solution of **tp-BDP** (171 mg, 0.2 mmol) in dichloromethane (15 mL) was dropwise added $FeCl_3$ (113 mg, 0.70 mmol) in CH_3NO_2 (1 mL). The reaction mixture was stirred at room temperature for 10 minutes, and was quenched by adding saturated aqueous solution of $NaHCO_3$. The reaction mixture was diluted with dichloromethane, washed twice with water (100 ml), dried over anhydrous Na_2SO_4, and evaporated under vacuum. The residue was purified by column chromatography on silica gel with CH_2Cl_2/Ethyl acetate (DCM/EA, 20/1, v/v) as eluent to give the desired **pf-BDP** in 45% isolated yield (76.5 mg). ^{1}H NMR (300 MHz, $CDCl_3$) δ 9.19 (s, 2H), 7.72 (s, 2H), 7.66 (s, 2H), 7.61 (s, 2H), 7.15 (s, 2H), 7.13 (s, 2H), 4.20 (s,6H), 4.17 (s, 6H), 4.10 (s, 6H), 4.03 (s, 6H), 2.52 (s, 3H), 2.29 (s, 6H). HRMS (APCI) calcd. for $C_{50}H_{45}BF_2N_2O_8$ $[M + H]^+$ 851.3310, found 851.3330.

4. Photophysical data

Table S1. Photophysical properties of **tp-BDP** and **pf-BDP** in different solvents at room temperature

dyes	solvents	λ_{max} (nm)	ε^a	λ_{em} (nm)	Φ^b	Stokes-shift (cm^{-1})
tp-BDP	Cyclohexane	633	108000	678	0.37	1049
	Toluene	640	107000	692	0.24	1174
	CH_2Cl_2	627	106000	687	0.13	1393
	THF	633	106000	691	0.13	1326
	MeCN	620	105000	682	0.09	1466
pf-BDP	Cyclohexane	840	271000	-	-	-
	Toluene	724	112000	752	0.04	514
	CH_2Cl_2	715	110000	769	<0.01	982
	THF	716	110000	759	<0.01	791
	MeCN	710	109000	753	<0.01	804

[a]Molar extinction coefficients are in the maximum of the highest peak. [b]The fluorescence quantum yields (Φ) of **tp-BDP** were calculated using Cresyl violet perchlorate in anhydrous methanol (Φ = 0.54) as the standard.[1] The fluorescence quantum yields of **pf-BDP** were calculated using 1,7-diphenyl-3,5-di(*p*-methoxyphenyl)-azadipyrromethene in trichloromethane (Φ = 0.36) as the standard.[2]

5. Absorption and emission spectra of dyes

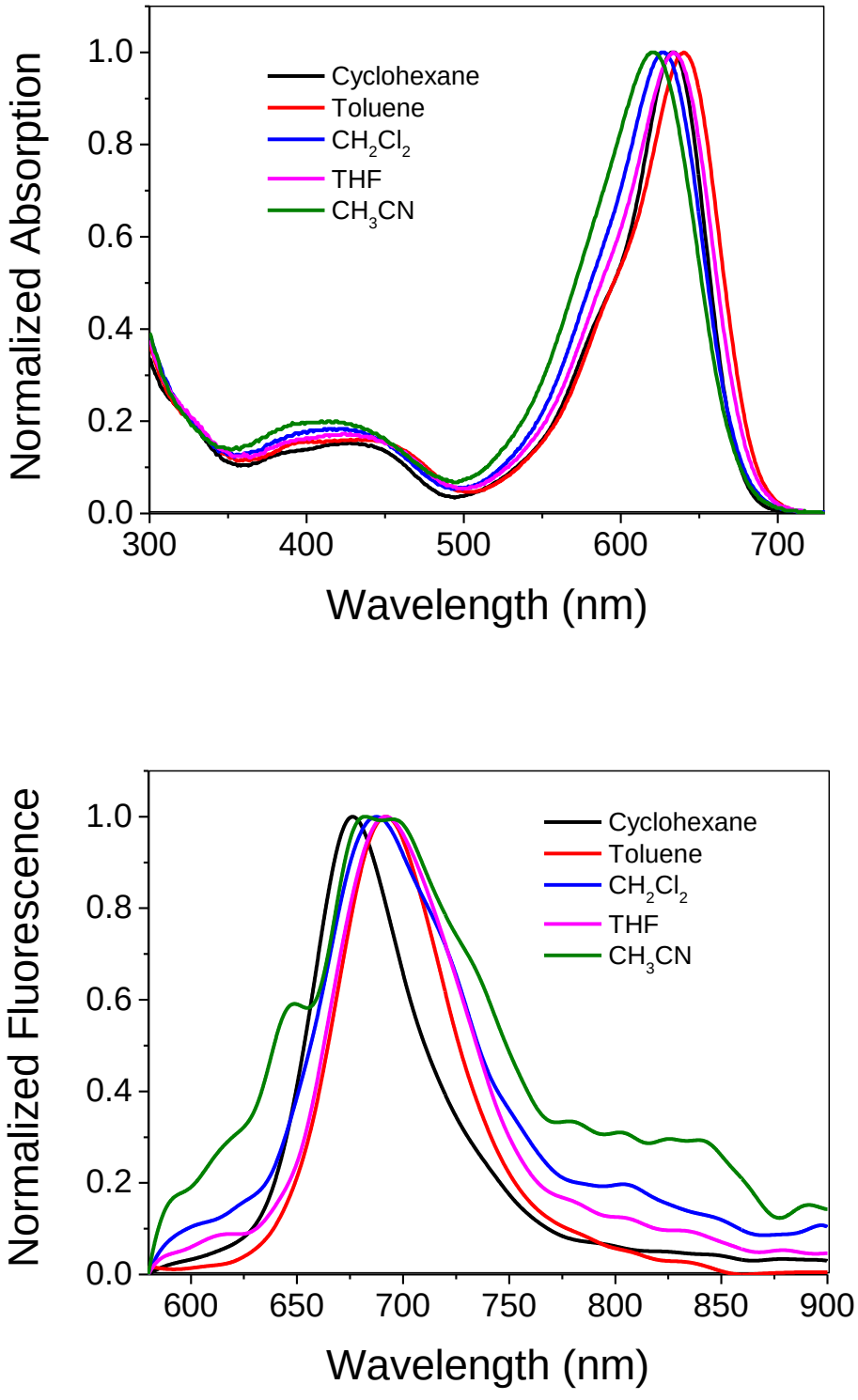

Figure S2. Absorption (top) and emission (bottom) spectra of **tp-BDP** recorded in different solvents. Excited at 570 nm.

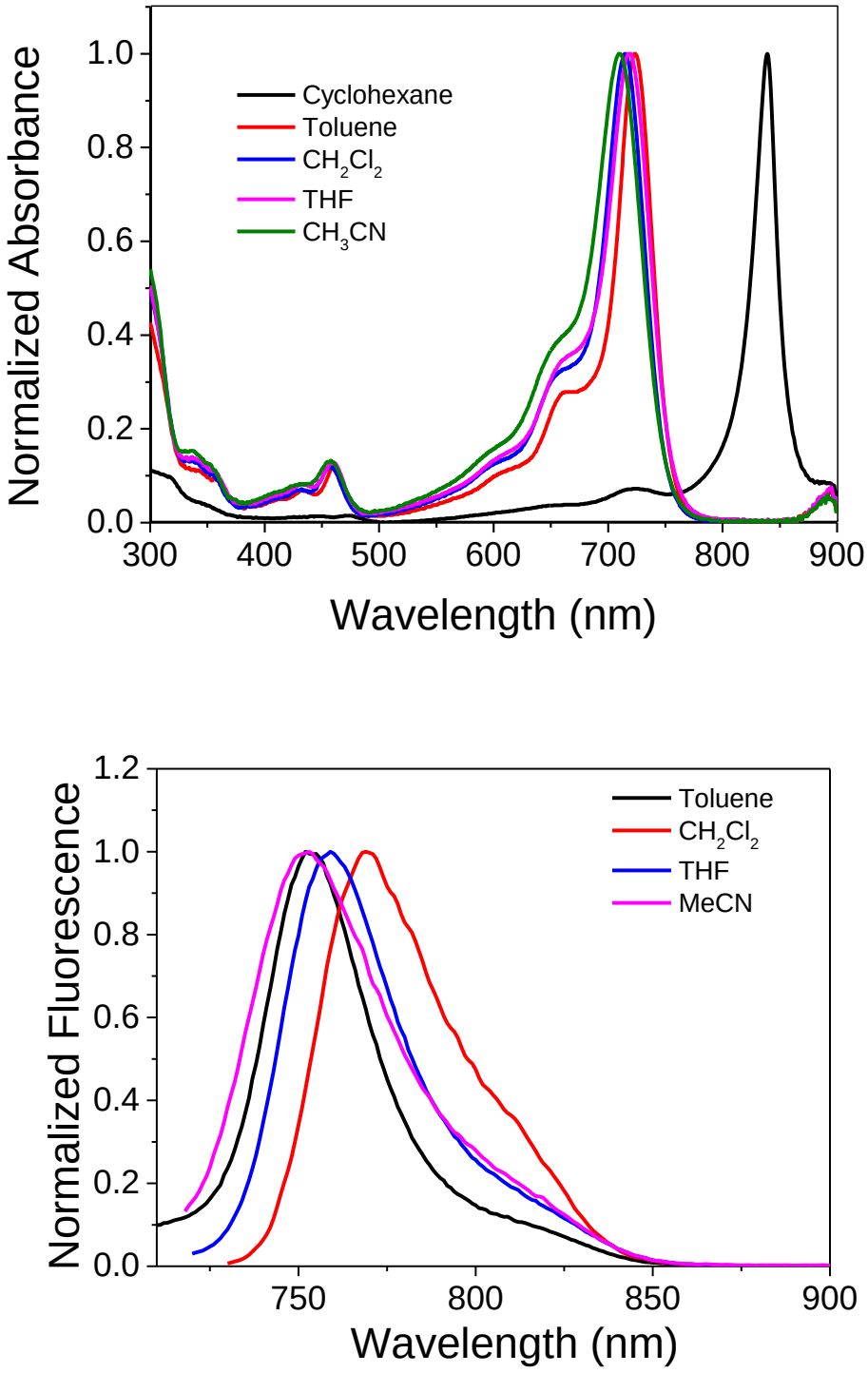

Figure S3. Overlaid normalized absorbance (top) and emission (bottom) spectra spectra of **pf-BDP** recorded in different solvents.

6. Electrochemical data of tp-BDP and pf-BDP

Cyclic voltammograms of **tp-BDP** and **pf-BDP** were measured in dichloromethane solution, containing 0.1 M $TBAPF_6$ as the supporting electrolyte, glassy carbon electrode as a working electrode, Pt wire as a counter electrode, and saturated calomel electrode (SCE) as reference electrode at 100 mV s^{-1} of scaning rate at room temperature.

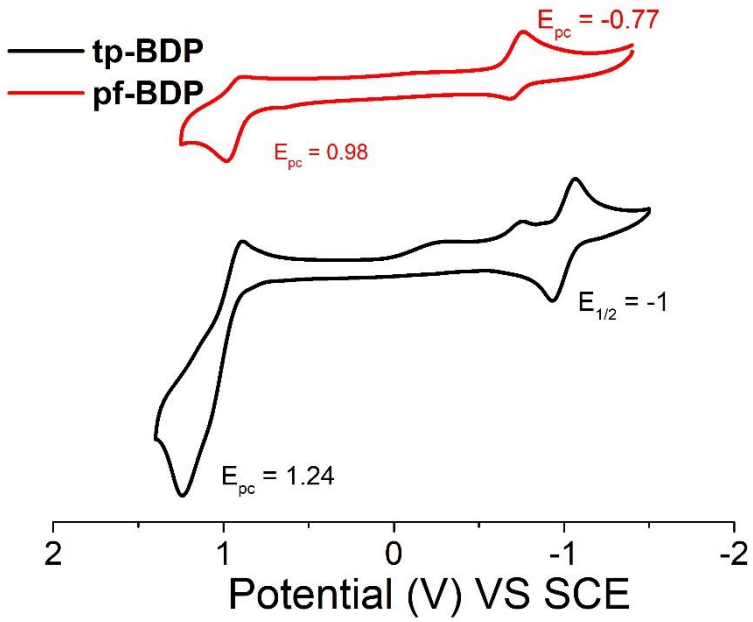

Figure S4. Cyclic voltammograms of 1 mM **tp-BDP** (black), **pf-BDP** (red) measured in dichloromethane solution, containing 0.1 M $TBAPF_6$ as the supporting electrolyte at room temperature. Glassy carbon electrode as a working electrode, and the scan rate at 100 mV/s.

Table S2. Electrochemical data acquired at 100 mV/s, and HOMO-LUMO Gaps determined from spectroscopy of dyes **tp-BDP** and **pf-BDP**.[a]

dyes	$E^o_{B/B^{-\cdot}}$ (V)	E_{p1}^{red} (V)	E_{red}^{onset} (V)	$E^o_{B^{+\cdot}/B}$ (V)	E_{p1}^{ox} (V)	E_{ox}^{onset} (V)	LUMO (eV)	HOMO (eV)	E_g^e (eV)
tp-BDP	-1.00	-	-0.88	-	1.24	0.85	-3.52	-5.25	1.73
pf-BDP	-	-0.77	-0.63	-	0.98	0.78	-3.77	-5.15	1.38

[a] E_{p1}^{red} = irreversible reduction peak potentials; $E^o_{B/B^{-\cdot}}$ = reversible reduction potential; E_{p1}^{ox} = irreversible oxidation peak potentials; $E^o_{B^{+\cdot}/B}$ = reversible oxidation potential; E_{red}^{onset} = the onset reduction potentials; E_{ox}^{onset} = the onset oxidation potentials; E_{LUMO} = -e(E_{red}^{onset} + 4.4); E_{HOMO} = -e(E_{ox}^{onset} + 4.4); E_g^e = bandgap, obtained from the intercept of the electrochemical data; $E_g^e = E_{LUMO} - E_{HOMO}$.

7. *J*-aggregates preparation and studies

Temperature-dependent *J*-aggregates preparation at different temperature in *n*-octane: pf-BDP in $CHCl_3$ solution (300 μM or 100 μM) were used as mother solution. A certain amount of corresponding volumes (30 μL) of the mother solution were transferred into another PVC tube. Then different temperatures (0 °C, 40 °C, 50 °C, 70 °C and 90 °C) of *n*-octane (3 mL) was added slowly first and then faster into the tube and was shaken upside down, respectively. After that, the mixture was scanning by UV-vis spectrophotometer immediately and recorded absorption spectra, respectively (Fig. S5).

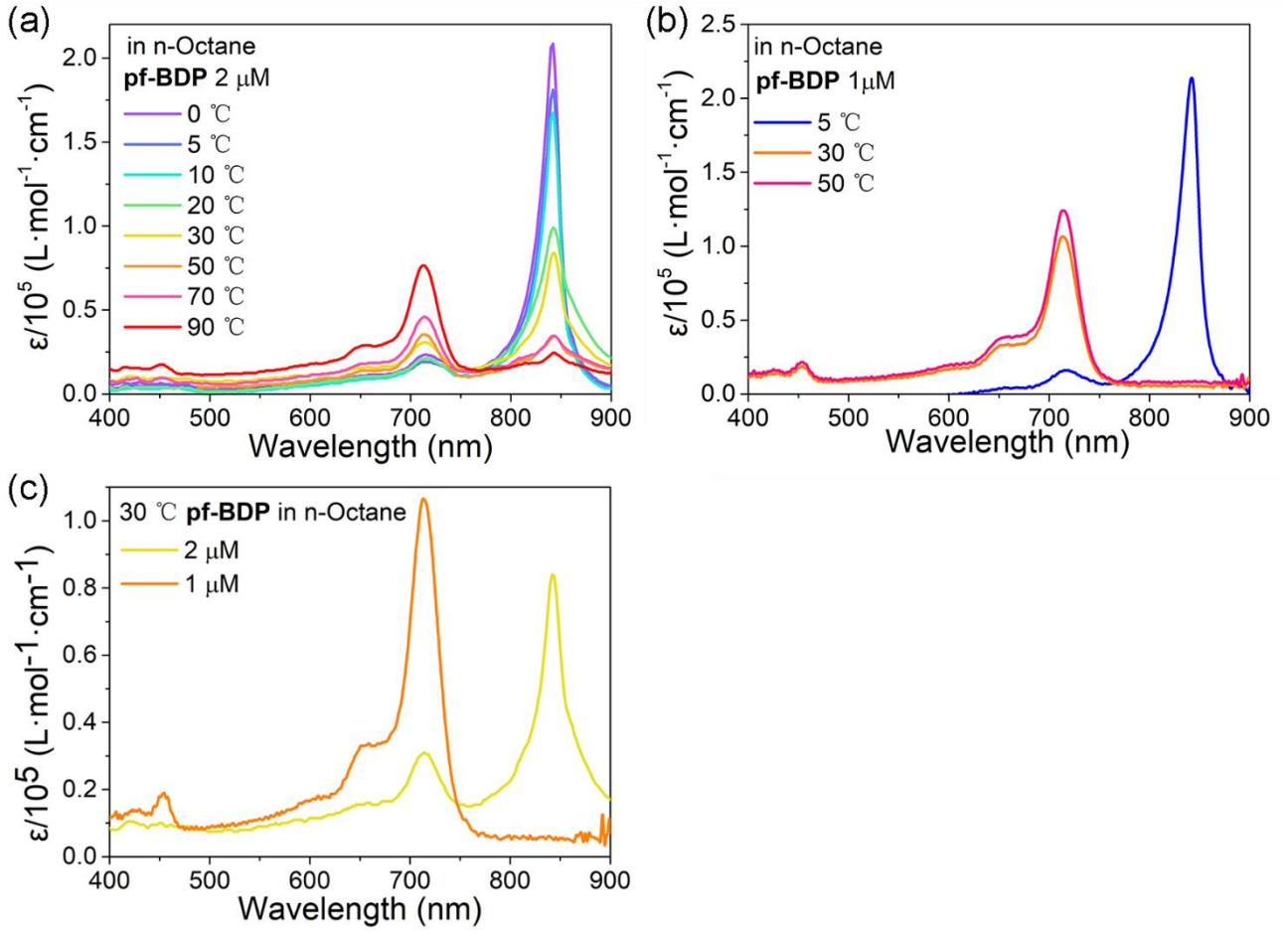

Figure S5. (a) Absorptions of temperature-dependent **pf-BDP** *J*-aggregates (2 μM) which were prepared at different temperatures in *n*-octane; (b) Absorptions of temperature-dependent **pf-BDP** *J*-aggregates (1 μM) which were prepared at different temperatures (0 °C, 30 °C and 50 °C) in *n*-octane. (c) Absorptions of **pf-BDP** *J*-aggregates which were prepared at different concentration (1 μM, 2 μM) but at the same temperature (30 °C).

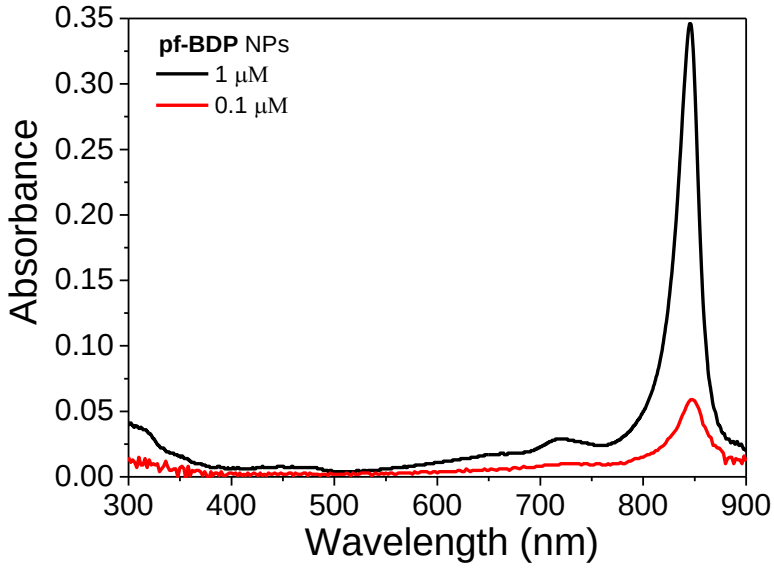

Figure S6. Absorption spectra of the **pf-BDP** *J*-aggregates diluted from 1 μM (balck line) to 0.1 μM (red line) by n-hexane solution at room temperature.

Absorption changes of *J*-aggregates with enhanced $CHCl_3$ volume: pf-BDP in $CHCl_3$ solution (100 μM, at 0 °C) were used as mother solution. A certain amount of corresponding volumes (30 μL, at 0 °C) of the mother solution were transferred into a 4 mL PVC tube. Then different volume fraction *n*-octane (at 0 °C) was added slowly first and then faster into the tube and shaken upside down. We diluted these *n*-octane mixtures with chloroform solution to 3 mL in the ice-water bath, at same time recorded the corresponding spectra respectively (Fig. S6).

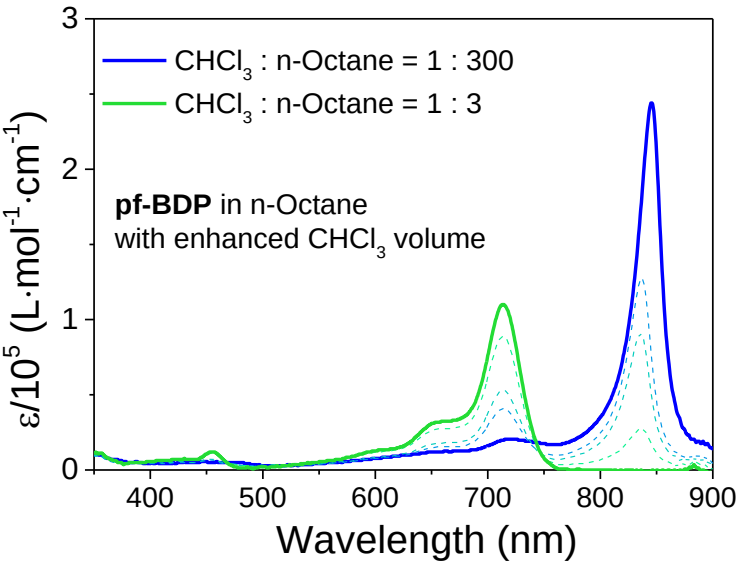

Figure S7. Absorption spectra of **pf-BDP** aggregates (1 μM) changed into monomer with gradually increased volume ratio of chloroform from 1:300 to 1:3 in *n*-octane.

Absorption changes of *J*-aggregates with raising temperature: pf-BDP *J*-aggregates were prepared by the above steps at 0 °C in a 4 mL PVC tube. Then these *J*-aggregates were warmed from 0 °C to 90 °C gradually in hot water bath. We recorded the temperature of the mixture and the corresponding absorption spectra, respectively (Fig. S7).

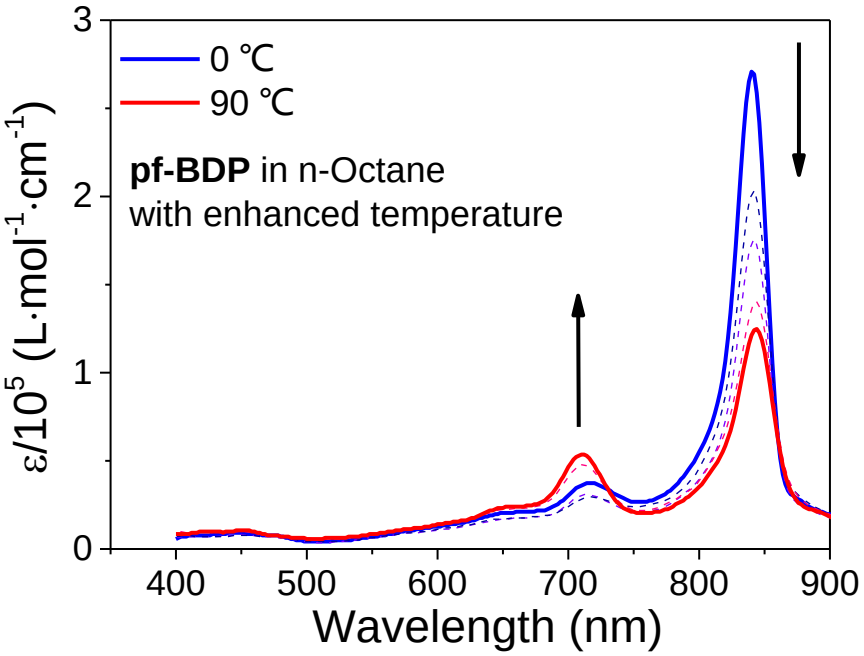

Figure S8. Absorption spectra of **pf-BDP** aggregates (1 μM) in *n*-octane which was recorded over the temperature range from 90 °C to 0 °C.

Absorption changes of pf-BDP with descended temperature: A *n*-octane solution of **pf-BDP** mixture (1% $CHCl_3$) were prepared by the above steps at 90 °C in a 4 mL PVC tube. We recorded the absorption spectra immediately and observed hardly *J*-aggregates formed at 90 °C. Then the PVC tube was gradually cooled to room temperature (25 °C). We recorded these absorption spectrums of the cooling period (Fig. S8).

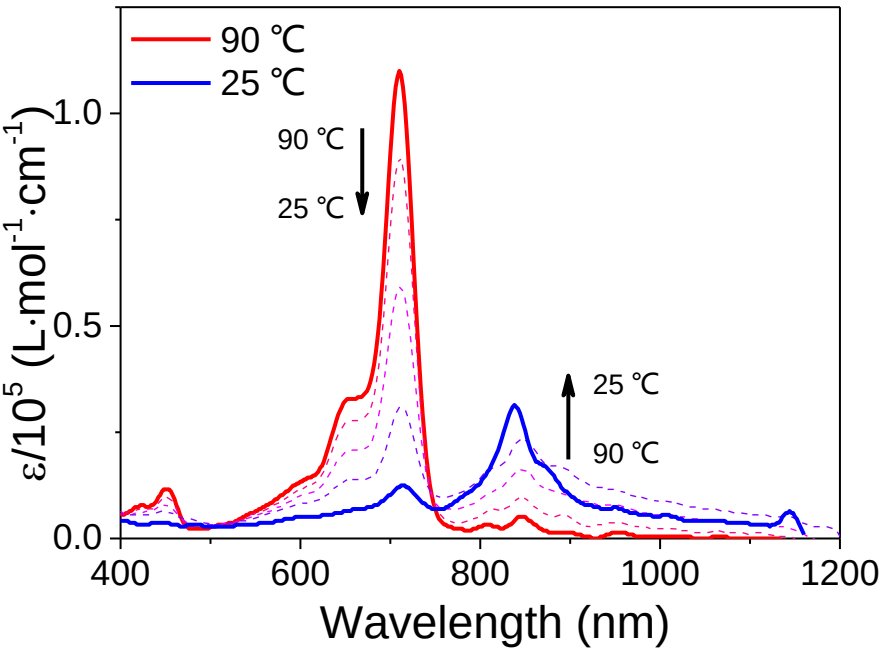

Figure S9. Absorptions of **pf-BDP** (2 μM) which were prepared at 90 °C (red) in *n*-octane and were gradually cooled to 25 °C (blue).

Preparation of pf-BDP *J*-aggregates in tetrahydrofuran (THF) & water system: pf-BDP in tetrahydrofuran solution (100 μM) was used as mother solution. A certain amount of corresponding volumes (30 μL) of the mother solution was dissolved in another tetrahydrofuran solution (0, 300, 450, 900, 1050 or 3000 μL) in a PVC tube. Then deionized water (at room temperature, total volume 3 mL) was added slowly first and then faster into the tube and was shaken upside down. The absorption spectra of **pf-BDP** *J*-aggregates in different proportions of THF & water mixture were recorded respectively (Fig. S9).

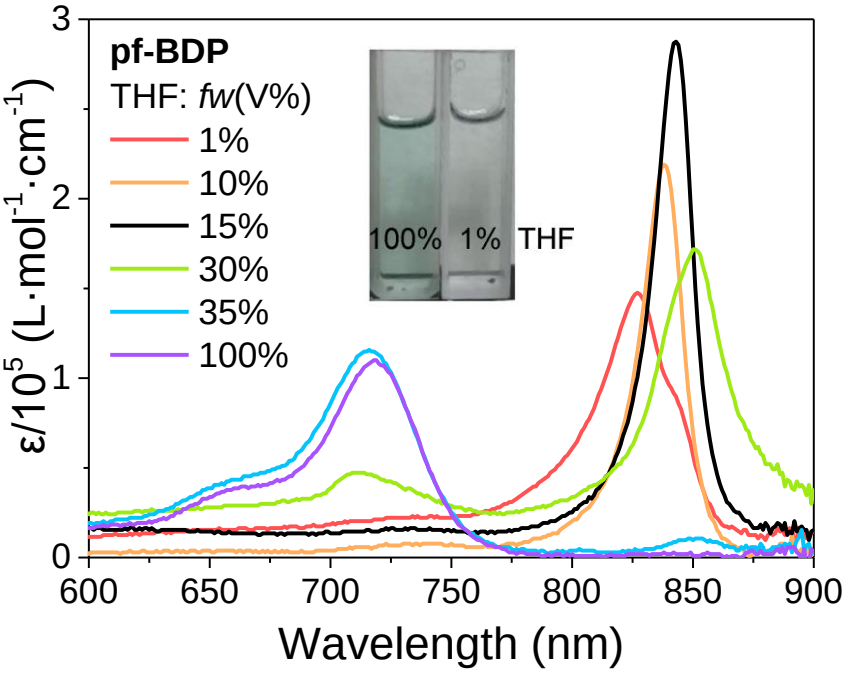

Figure S10. Absorption of **pf-BDP** (1μM) in mixed solvents at room temperature. (V% represents the volume ratio of tetrahydrofuran to water)

pf-BDP *J*-aggregates preparation at different temperature in THF & water system: pf-BDP in tetrahydrofuran solution (100 μM) was used as mother solution. A certain amount of corresponding volumes (30 μL) of the mother solution was transferred into a PVC tube. Then different temperatures (0°C, 40 °C, 50 °C, 70 °C and 90 °C) of *n*-octane (2970 μL) was added slowly first and then faster into the tube and was shaken upside down, respectively. After that, the mixture was scanning by UV-vis spectrophotometer immediately and recorded absorption spectra, respectively (Fig. S10).

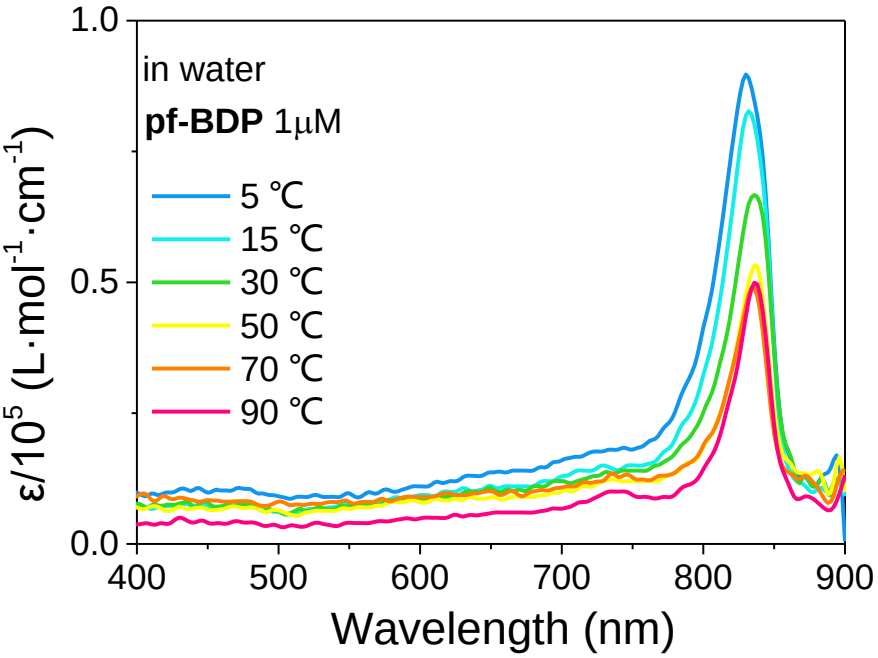

Figure S11. Absorptions of **pf-BDP** *J*-aggregates (1 μM) which were prepared at different temperatures (0 °C, 15 °C, 30 °C, 50 °C, 70 °C and 90 °C) in THF & water mixture. Spectrums were recorded immediately after preparation at the same temperature indicated above.

N-E model for pf-BDP *J*-aggregates:

Using similar methods as previously reported,[8-10] the molar extinction coefficient values of the monomeric (ε_{mon}) and aggregated (ε_{agg}) species in Fig. S13b were estimated from their respective absorption spectra, ε(T) is the apparent absorption coefficient at the given temperature, and the fraction of aggregation was calculated as following:

$$\alpha_{agg}(T) = 1 - \frac{\varepsilon(T) - \varepsilon_{agg}}{\varepsilon_{mon} - \varepsilon_{agg}} \qquad \text{eq S2}$$

The fractions of aggregated species (α_{agg}) in the elongation and nucleation regimes (N-E model) were then fitted to equations S3 and S4, respectively: [8-11]

As $T < T_e$, elongation regime:

$$\alpha_{agg} = \alpha_{SAT}\left[1 - \exp\left(\frac{-\Delta H_e}{RT_e^2}(T - T_e)\right)\right] \qquad \text{eq S3}$$

α_{SAT} is a parameter introduced to ensure that α_{agg} / α_{SAT} does not exceed unity, ΔH_e (J mol^{-1}) is the enthalpy release of elongation process, R is the ideal gas constant (8.314 J mol^{-1} K^{-1}), T_e (international standard unit: K) the elongation temperature. Fitting the experimental data to the elongation regime (eq S3) using 1st opt software to calculate ΔH_e and T_e.

As T > Te, nucleation regime:

$$\alpha_{agg} = {K_a}^{1/3}\exp\left[\left(\frac{2}{3}{K_a}^{-\frac{1}{3}} - 1\right)\frac{\Delta H(T - T_e)}{RT_e^2}\right] \qquad \text{eq S4}$$

K_a is the dimensionless equilibrium constant of the activation step at the elongation temperature; ΔH (J mol^{-1}) is the enthalpy release. Fitting the experimental data to the nucleation regime (eq S) using 1st opt software to calculate ΔH and K_a.

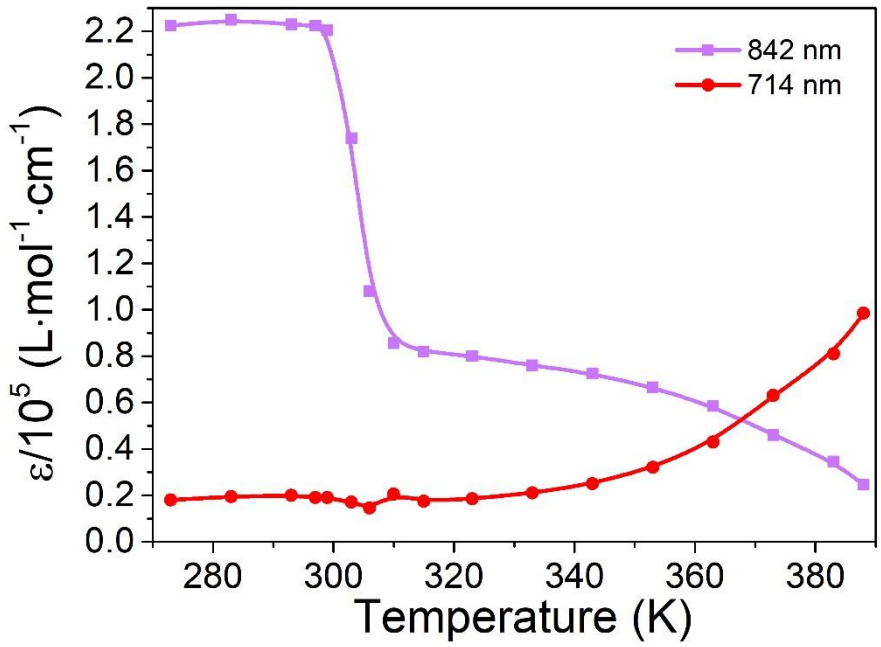

Figure S12. Molar extinction coefficient changes at 842 nm (purple, *J*-band) and 714 nm (red, monomer) for **pf-BDP** at 2 μM in $CHCl_3$/*n*-octane (1:99, v/v) which was recorded over the temperature range from 0 °C (273 K) to 115 °C (388 K).

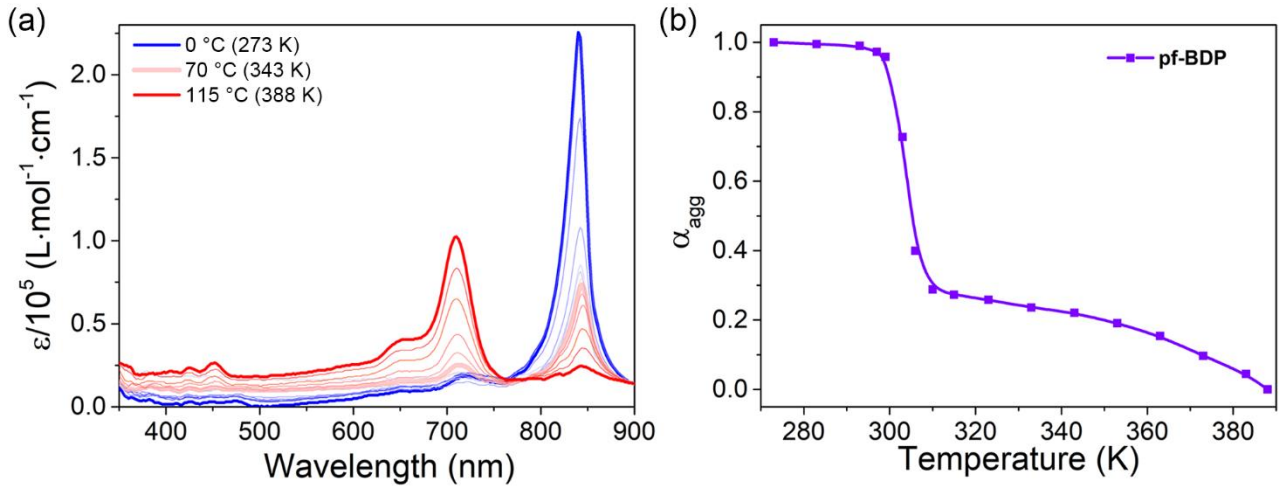

Figure S13. (a) Absorption spectra of **pf-BDP** aggregates (2 μM) in $CHCl_3$/*n*-octane (1:99, v/v) which was recorded over the temperature range from 0 °C (273 K) to 115 °C (388 K). (b) The calculated fraction of *J*-aggregate (α_{agg}) of **pf-BDP** as a function of temperature based on the absorption coefficient change at 842 nm and 714 nm of **Fig. S12** using equations S2.[8-10]

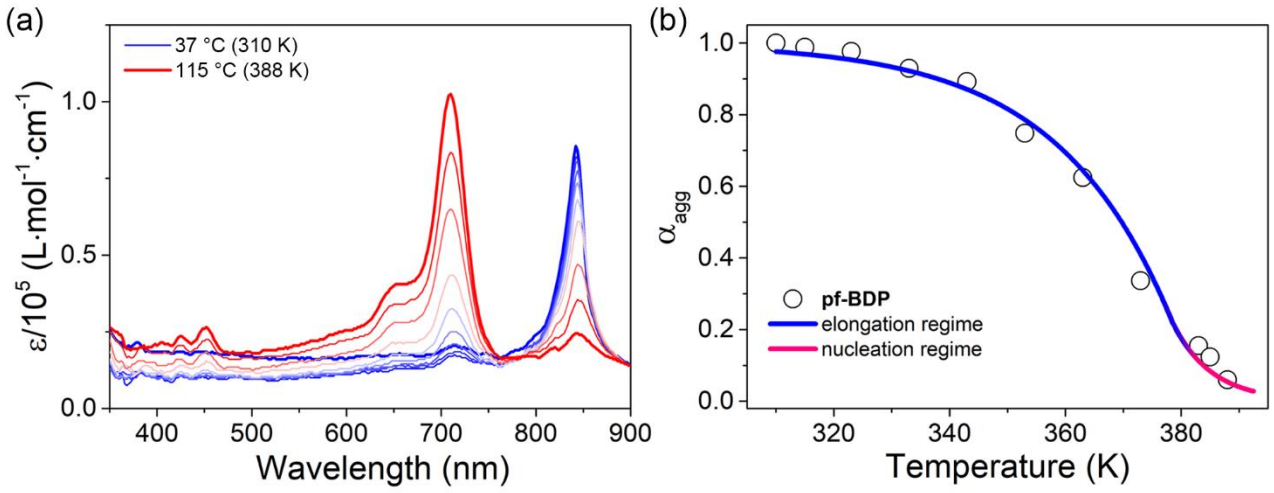

Figure S14. (a) Absorption spectra of **pf-BDP** aggregates (2 μM) in *n*-octane in $CHCl_3$/*n*-octane (1:99, v/v) which was recorded over the temperature range from 37 °C (310 K) to 115 °C (388 K). (b) The calculated fraction of *J*-aggregate (α_{agg}) of **pf-BDP** as a function of temperature based on the absorption coefficient change at 842 nm and 714 nm (Figure S13a); the red lines are the fits in the elongation and nucleation regimes to the N-E model using equations S3 and S4, respectively($\Delta He = -47.6$ kJ mol^{-1}, $K_a = 0.0034$).[8-10]

The size of coherent domain in the aggregate: [12]

$$N_{J-agg} = \left(\frac{\mathrm{Fwhm}_{mon}}{\mathrm{Fwhm}_{agg}}\right)^2 \qquad \text{eq S5}$$

Fwhm is the halfwidth of absorption peak.

Calculations of transition dipole moments:[10, 13-14]

$$\mu_{eg}{}^2 = \frac{3hc\varepsilon_0 \cdot \ln(10) \cdot 9n}{2000\pi^2 \cdot N_{AV} \cdot (n^2+2)^2} \cdot \int \frac{\varepsilon(\tilde{\nu})d\tilde{\nu}}{\tilde{\nu}} \qquad \text{eq S6}$$

Transition dipole moments were obtained from equation eq S6 with *h* being Planck's constant (6.6262 x 10^{-34} Js), c is the speed of light (2.9979 x 10^{10} cm·s^{-1}), ε_0 is the electric field constant (8.8542 x 10^{-23} J·K^{-1}), n is the refractive index of the solvent, N_{AV} is the Avogadro constant (6.0221 x 10^{-23} Js) and $\tilde{\nu}$ (cm^{-1}) is the attenuation coefficient as a function of the wavenumber $\tilde{\nu}$.

8. Preparation of pf-BDP nanoparticles (pf-BDP NPs)

pf-BDP NPs were fabricated following literature procedures.[15-16] Compound **pf-BDP** (654 μL, 900.6 μM in chloroform) and F127 (8 mL, 12.5 mg mL^{-1} in chloroform) were added into a flask with 5 mL chloroform. And the mixture sonicated for 20 min at room temperature. The chloroform was evaporated entirely under reduced pressure, after that, water or 1640 complete medium (5 mL) was added and shaken. Finally, the liquid was stored at 4 °C for further experiments.

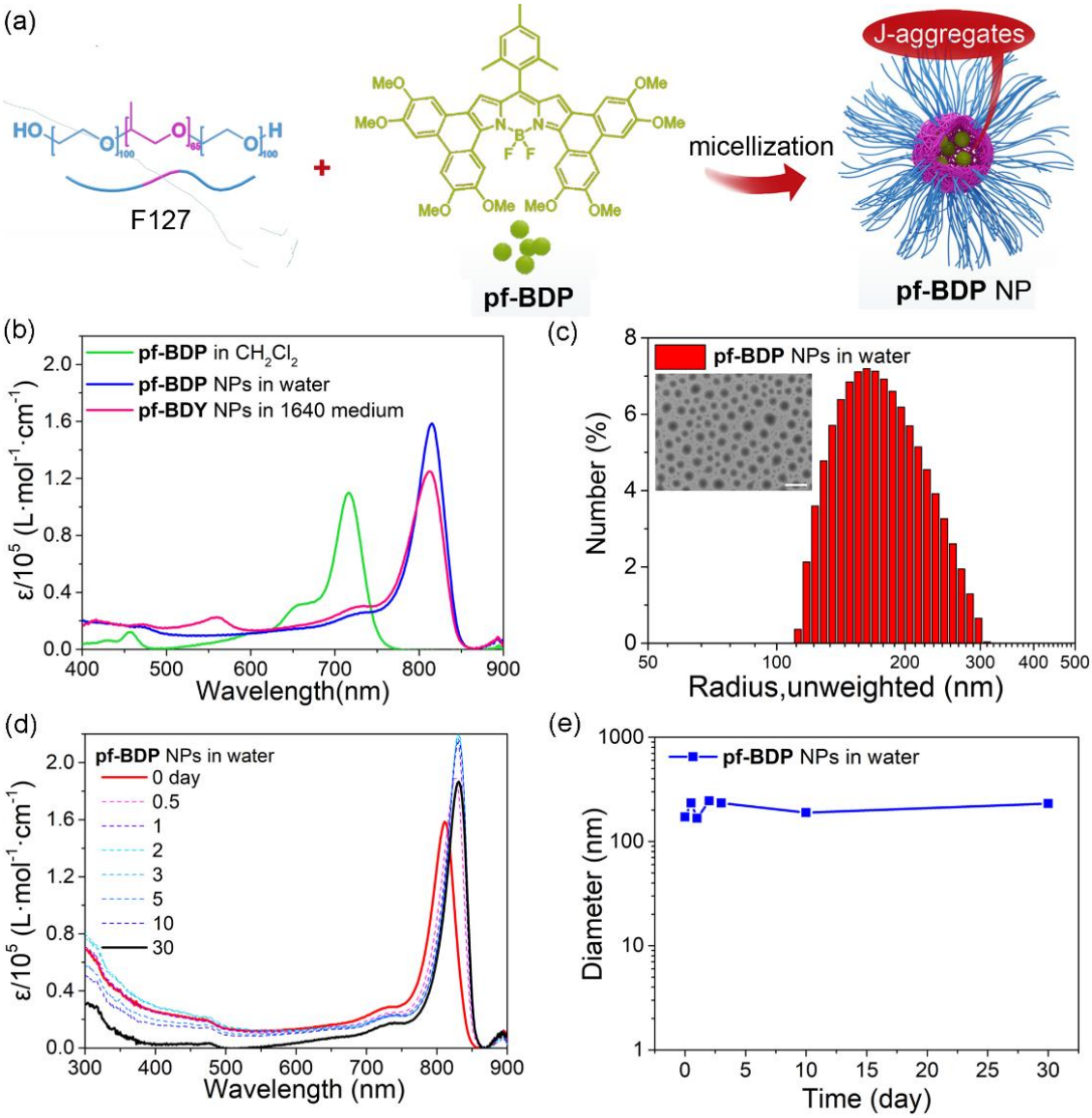

Figure S15. (a) A schematic illustration of the self-assembled nanoparticles of **pf-BDP** J-aggregates and F127 surfactants; (b) Absorption spectra of **pf-BDP** monomer in CH_2Cl_2 (green), pf-BDP NPs in deionized water (blue) and in RPMI-1640 cell culture medium (pink) at concentration of 5 μM; (c) The hydrodynamic diameter of **pf-BDP** NPs in water via DLS and TEM images of **pf-BDP** NPs, scale bars = 500 nm; (d) Absorption spectra of **pf-BDP** NPs dispersed in water recorded at different time intervals; (e) DLS size distribution of **pf-BDP** NPs dispersed in water recorded at different time intervals.

9. Photothermal activity and photothermal conversion efficiency

The **pf-BDP** NPs were irradiated with 808 nm laser at different intensity power at different concentration for a period of 720 s with individual F127 surfactant as blank control group. The concentrations of **pf-BDP** NPs we chose were 5 μg ml^{-1}, 10 μg ml^{-1}, 15 μg ml^{-1} and 20 μg ml^{-1}; the chosen different power densities of the 808 nm laser were 0.3 W cm^{-2}, 0.9 W cm^{-2}, 1.4 W cm^{-2} and 2.3 W cm^{-2}, and the used amount of **pf-BDP** NPs for each sample was 2 mL. We recorded the temperature at 10 s intervals, and calculated photothermal conversion efficiency according to the reference method.[17-18] Detailed calculation was given as following:

$$\eta = \frac{hA\,\Delta T_{max,NPs} - Q_s}{I(1 - 10^{-A_\lambda})} \qquad \text{eq S7}$$

where h is the heat transfer coefficient; A is the surface area of the container, and hA can be determined by eq S8. $\Delta T_{max,NPs}$ is the temperature change of the **pf-BDP** NPs dispersion at the maximum steady state temperature ; I is the laser power; A_λ is the absorbance of **pf-BDP** NPs at the wavelength of 808 nm, and η is the conversion efficiency from the absorbed light energy to thermal energy. Q_s is heat associated with the light absorbed by solvent per second and can be determined by eq S11.

$$hA = \frac{\Sigma m_i C_{Pi}}{\tau_s} \qquad \text{eq S8}$$

where m and C_p are the mass and heat capacity of solvent (water), respectively; τ_s is the time constant can be determined according to the eq S9 and eq S10.

$$\tau_s = -\ln\theta \qquad \text{eq S9}$$

$$\theta = \frac{\Delta T}{\Delta T_{max,NPs}} \qquad \text{eq S10}$$

Where $\Delta T_{max,NPs}$ is the temperature change of the **pf-BDP** NPs dispersion at the maximum steady state temperature; ΔT is defined as T-Tsurr (T and Tsurr are the solution temperature and ambient temperature of the surroundings, respectively).

$$Q_s = \frac{c_{water} m_{water} \Delta T_{max,water}}{t} \qquad \text{eq S11}$$

Q_s is the heat associated with the light absorbance of the solvent, which is measured independently using pure water without **pf-BDP** NPs; $\Delta T_{max,water}$ is the temperature change of pure water; t is the irradiation time of the laser.

Thus, the photothermal conversion efficiency (η) of **pf-BDP** NPs could be calculated.

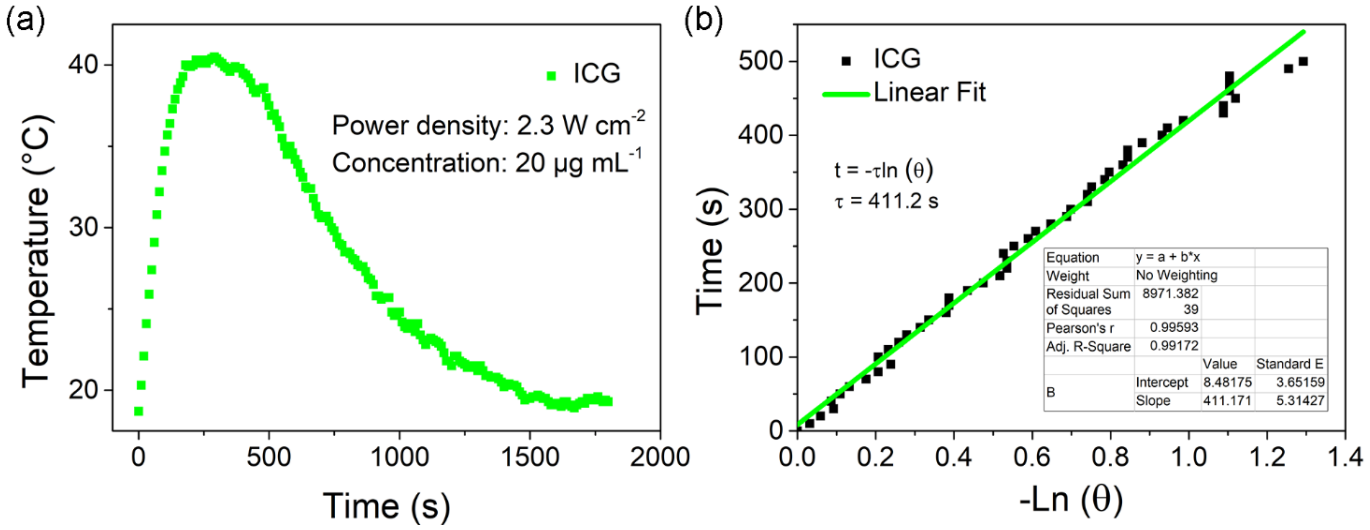

Figure S16. (a) Photothermal response of ICG aqueous solution which was turned off after irradiation by 808 nm laser for 480 s; (b) Plot of cooling time versus negative natural logarithm of the temperature obtained from the cooling stage of (a) and the photothermal conversion efficiency (η) = 18.7 %.

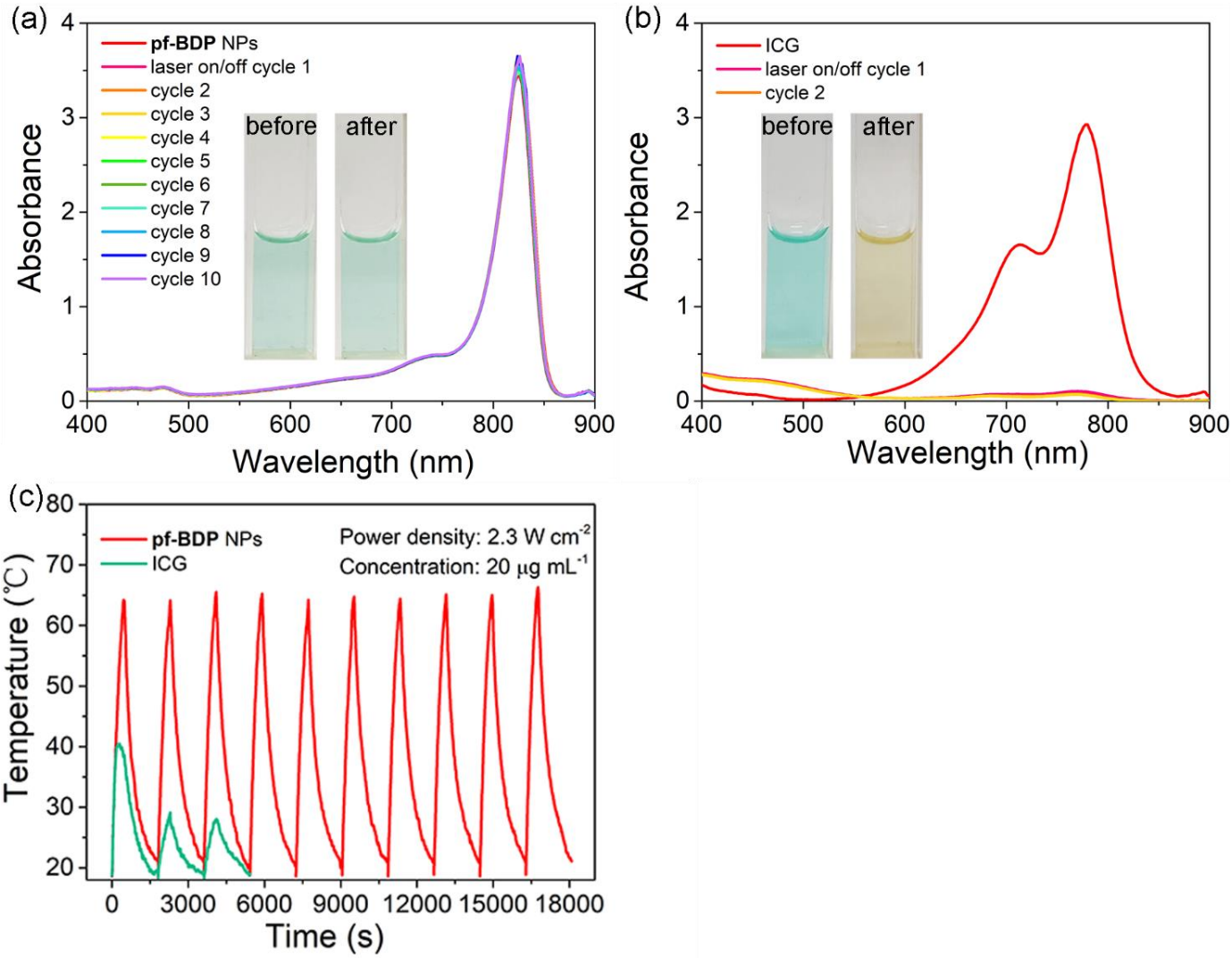

Figure S17. UV-vis-NIR absorbance spectra of **pf-BDP** NPs aqueous solutions (a, 20 μg/mL) and ICG monomer aqueous solutions (b, 20 μg/mL) before and after 10 cycles of photothermal heating irradiated with an 808 nm laser under the power of 2.3 W/cm^2. Insets are the photos before (left) and after (right) laser-induced photothermal heating. (c) Temperature evolutions of the **pf-BDP** NPs and ICG monomer aqueous solution under irradiation (2.3 W cm^{-2}) during 10 laser on/off cycles (480 s per cycle). 808 nm laser was used.

Preparation of ICG J-aggregation: ICG J-aggregates were prepared according to a previous reported method.[23] A mixture of ICG (5.75 mg, 1.15 mg/mL) in 5 mL water (in sealed Shrek tube) was heated in a digital dry baths at 90 °C (actual liquid temperature: 65 °C) while being stirred at 750 rpm for 3 days, and the formation of ICG *J*-aggregation was monitored with UV−vis−NIR spectroscopy.

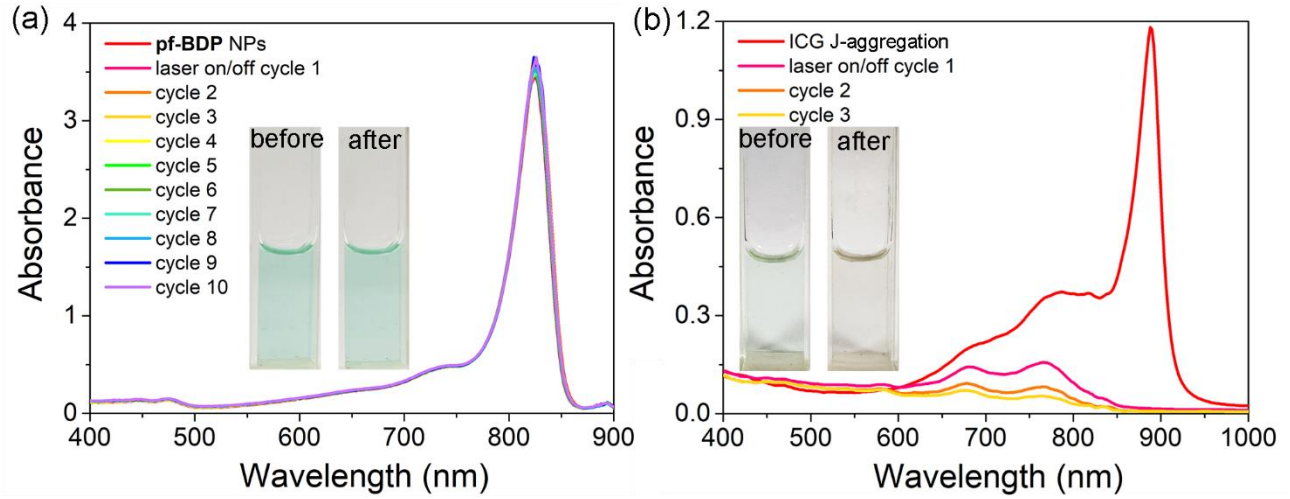

Figure S18. UV-vis-NIR absorbance spectra of **pf-BDP** NPs aqueous solutions (a, 20 μg/mL) and ICG J-aggregation aqueous solutions (b, 20 μg/mL) before and after 10 cycles of photothermal heating irradiated with a 808 nm laser under the power of 2.3 W/cm^2. Insets are the photos before (left) and after (right) laser-induced photothermal heating.

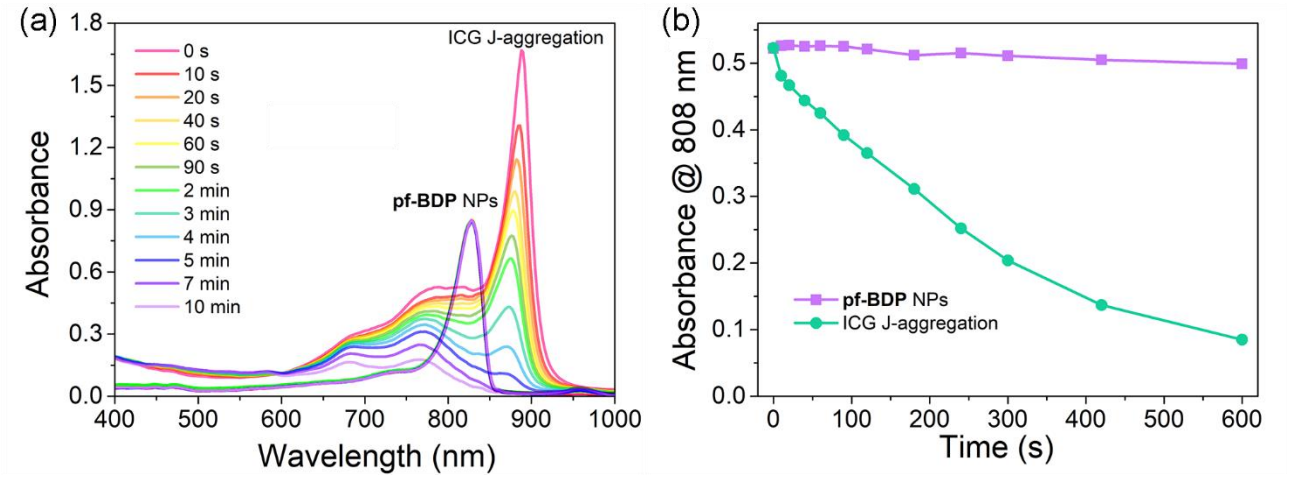

Figure S19. Absorption spectra (a) and absorption at 808 nm (b) of **pf-BDP** NPs and ICG *J*-aggregates solution changed as a function of time irradiated with an 808 nm laser under the power of 2.3 W/cm^2.

10. Cellular studies

Cell culture

Hela cells (human cervical cancer cells) were cultured in culture media (RPMI-1640, supplemented with 10% FBS and 1% penicillin/streptomycin solution) at 37 °C in an atmosphere of 5% CO_2 and 95% humidified atmosphere for 24 h.[19-20]

Photothermal cytotoxicity determined by the CCK-8 method.

The HeLa cells (7000) per well were seeded on 96-well plates and incubated in 1640 complete medium for 24 h at 37 °C. Then, a gradient concentration of **pf-BDP** NPs from 0 to 5 μg mL^{-1} in a fresh medium were added into the 96-well plate, and the cells with the NPs were incubated at 37 °C for 12 h. The experimental group of the cells were irradiated with an 808 nm laser (4.0 W cm^{-2}) for 6 min at room temperature. Then these cells were followed by a 12 h incubation solely in the dark (total 24 h) in the incubator. The control groups of the cells were incubated in the dark, for the duration of 24 h under identical experimental conditions except illumination. After that, the working solutions were then removed, and the cells were washed with PBS buffer cautiously for two times. A total of 10 μL of CCK-8 (Cell Counting Kit-8, BIOMIKY)[21] was added into each well, and the cells were further incubated at 37 °C for 1 h in a 5% CO_2 humidified atmosphere. The plate was shaken for 5 min, and the absorbance was measured at 450 nm using a microplate reader (Multiskan Sky).

Live–dead cell staining

Live–dead cell staining analysis was also performed to evaluate cell viability. [22] Briefly, a total of 30000 HeLa cells were seeded into a glass bottom dish and were cultured in culture media (RPMI-1640, supplemented with 10% FBS) at 37 °C in an atmosphere of 5% CO_2 and 95% humidified atmosphere for 24 h. Cells were dived into four groups. Cells in the first group were incubated in the incubator for 10 h (Fig 5c). Cells in the second group were treated with **pf-BDP** NPs (at a final concentration of 5 μg ml^{-1}) and were kept in the dark in the same condition for 10 h (Fig 5d). Cells in the third group were incubated for 6 h then illuminated for 5 min without the **pf-BDP** NPs, after that further incubation for another 4 h (total 10 h) (Fig 5e). Cells in the last group were incubated with **pf-BDP** NPs (5 μg ml^{-1}) for 6 h, then irradiated for 5 min after that further incubation for another 4 h (total 10 h) (Fig 5f). The cells were then washed with PBS twice and replaced with AO-PI mixture in the dark at room temperature. After 15 min, these plates were taken pictures immediately.

11. ^{1}H, ^{13}C NMR and HRMS spectra for all compounds

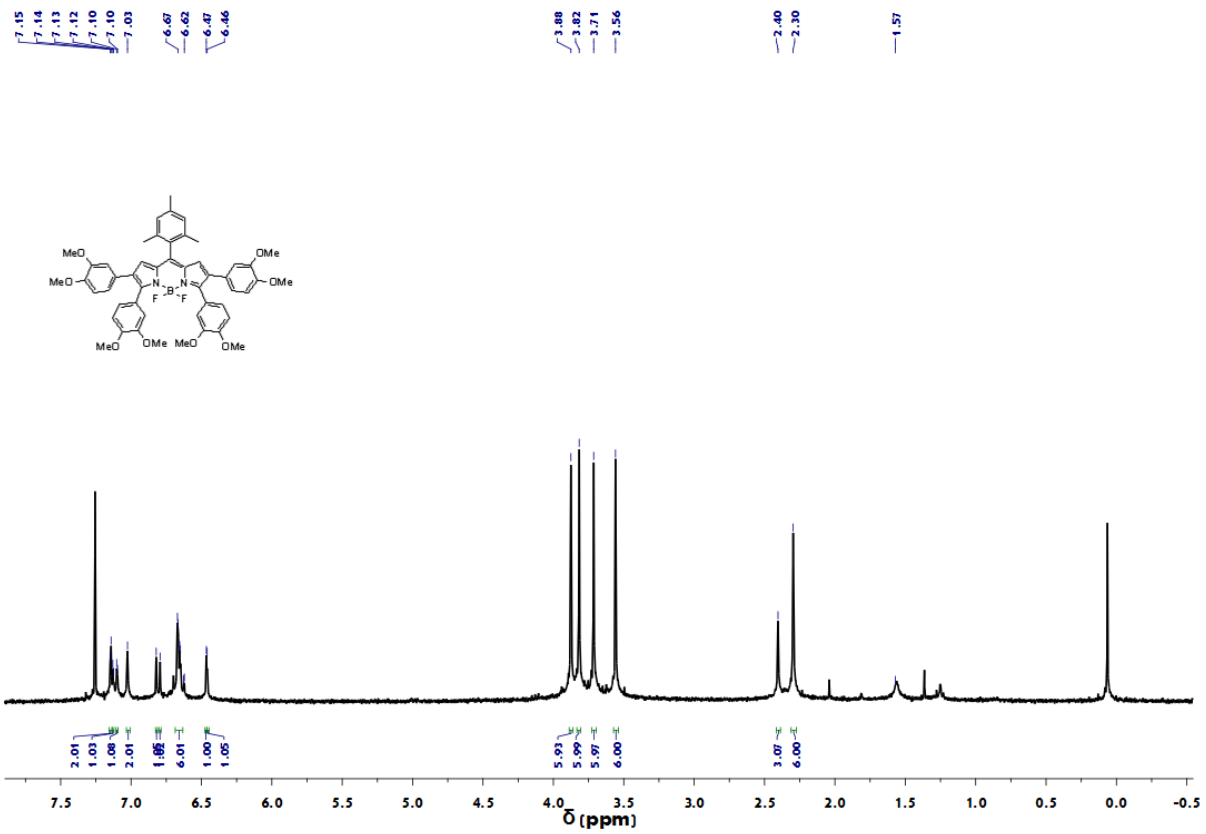

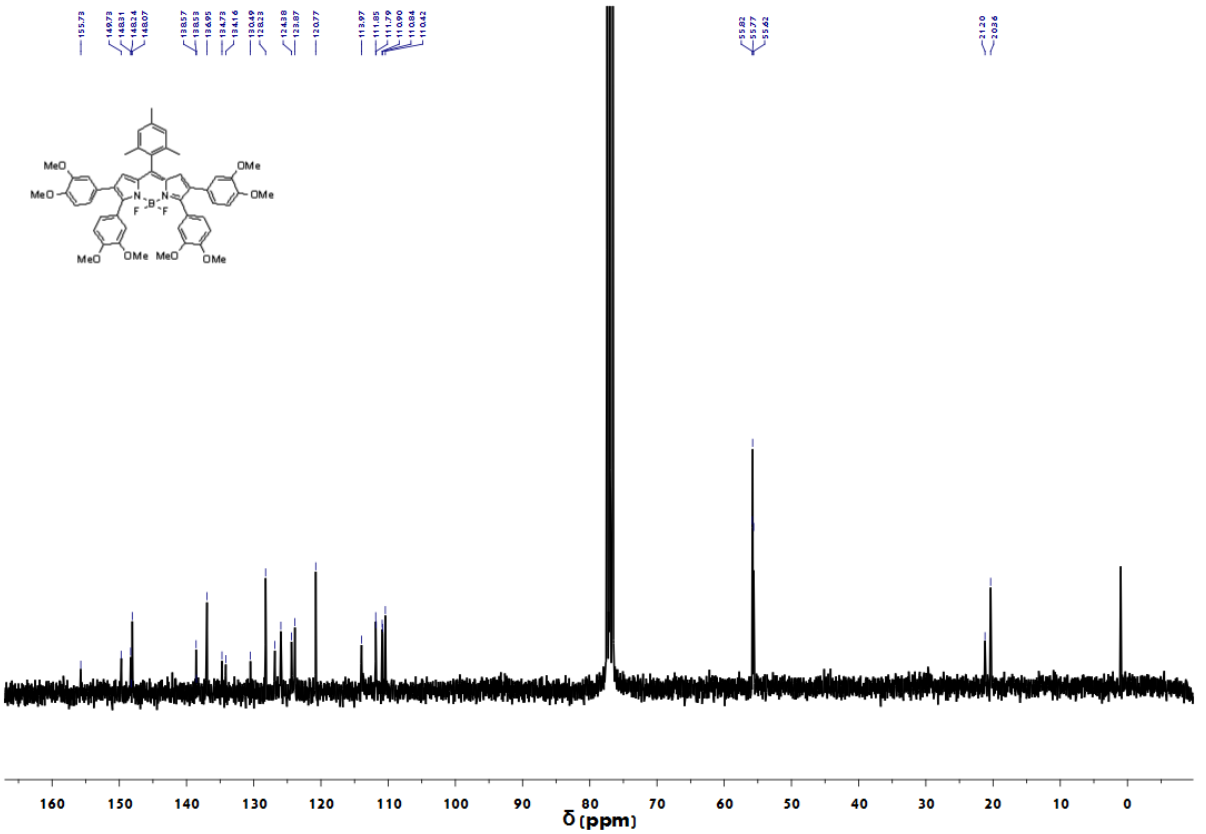

^{1}H NMR and ^{13}C NMR of compound **tp-BDP** in $CDCl_3$

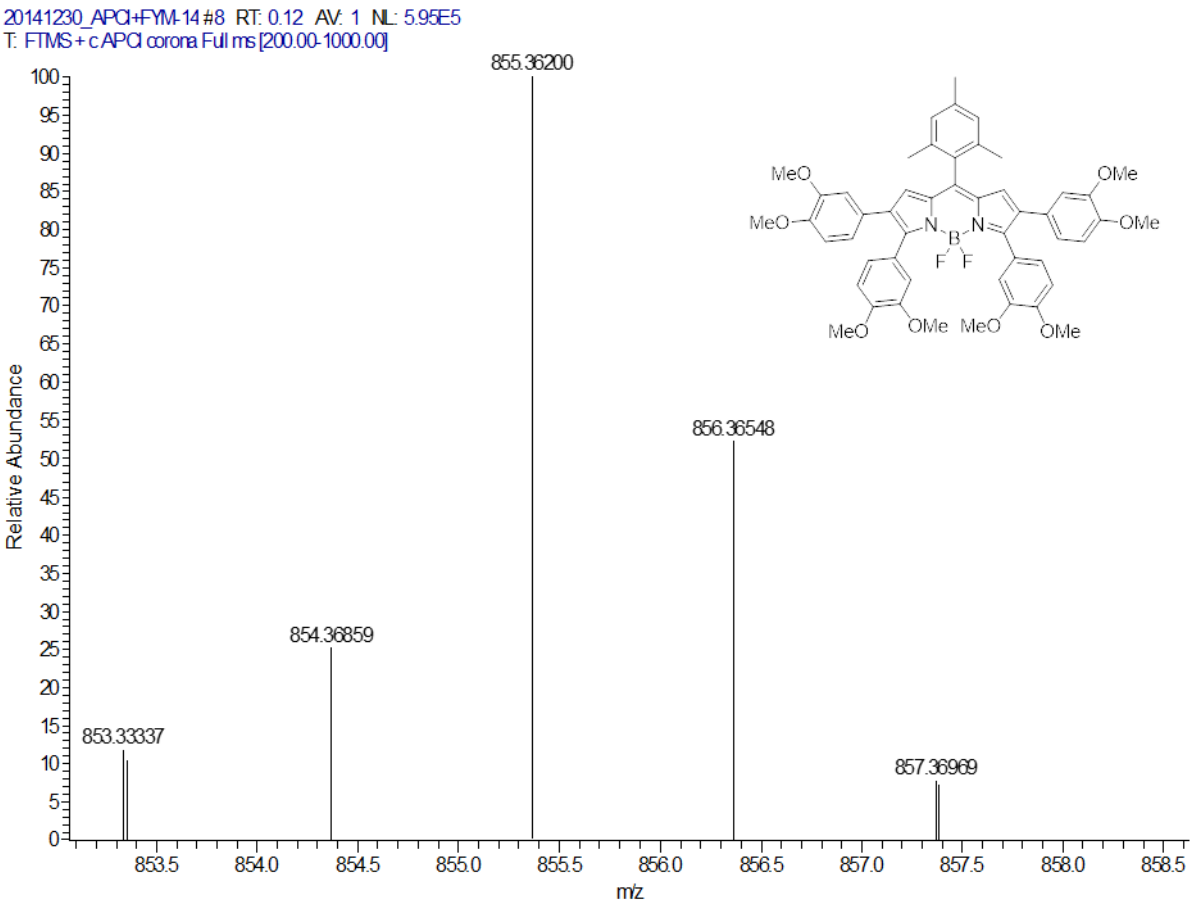

HRMS for **tp-BDP**

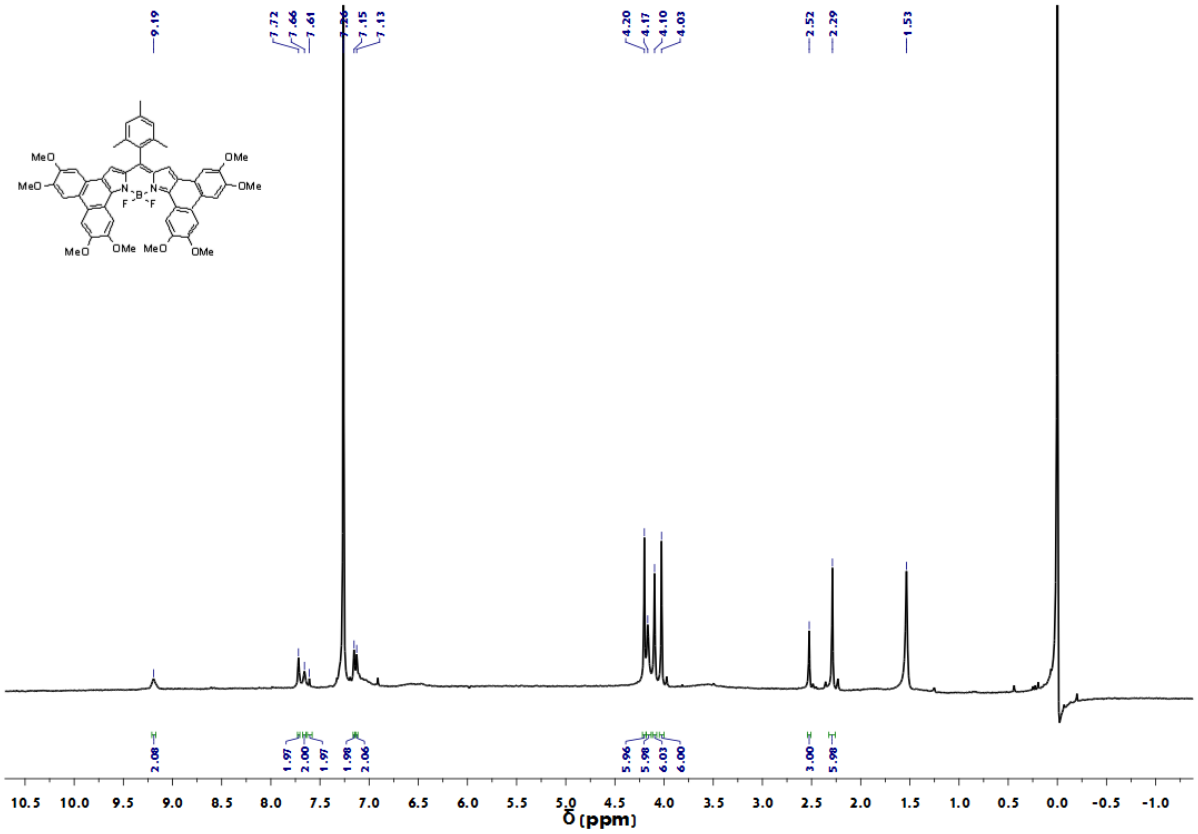

^{1}H NMR of compound **pf-BDP** in $CDCl_3$

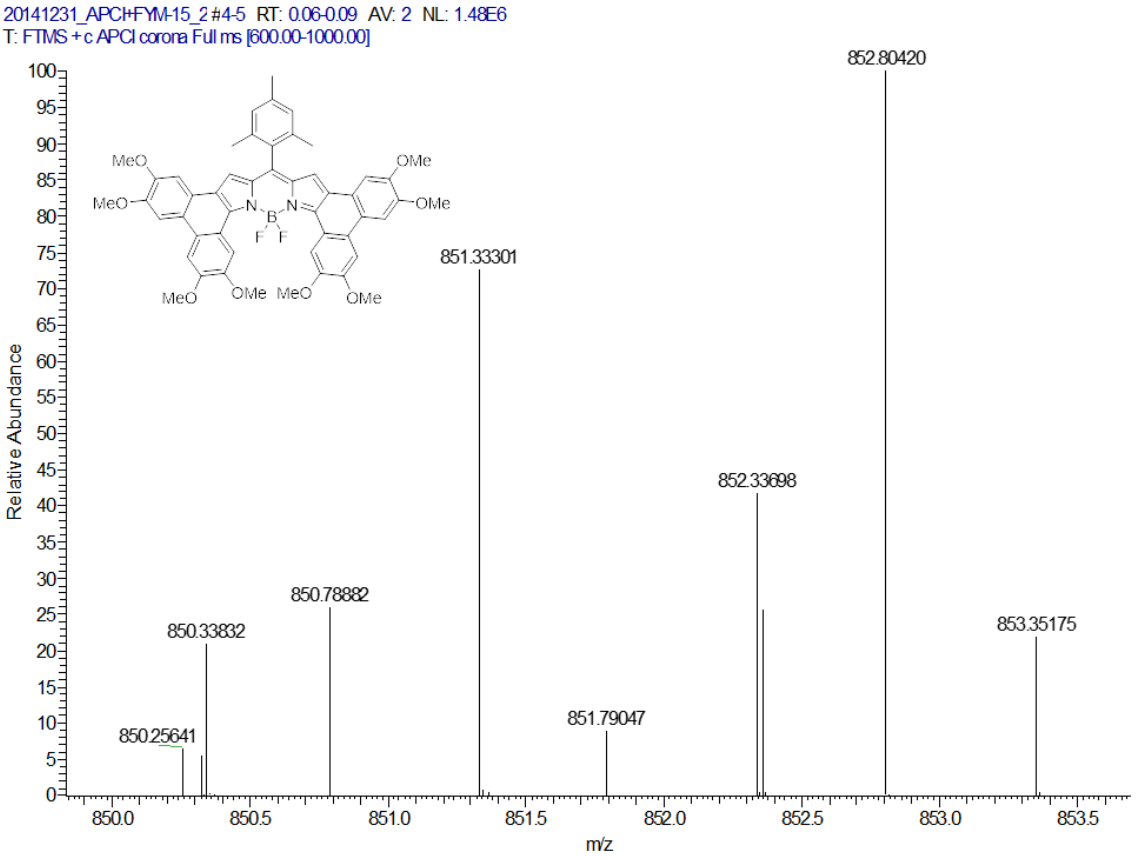

HRMS for **pf-BDP**

12. REFERENCES

1. S. J. Isak and E. M. Eyring, *J. Phys. Chem.*, 1992, **96**, 1738-1742.

2. S. O. McDonnell, M. J. Hall, L. T. Allen, A. Byrne, W. M. Gallagher and D. F. O'Shea, *J. Am. Chem. Soc.,* 2005, **127**, 16360-16361.

3. J. Killoran, L. Allen, J. F. Gallagher, W. M. Gallagher and D. F. O'Shea, *Chem. Commun.*, 2002, **33**, 1862.

4. X. Zhang, H. Wang, D. Li, M. Chen, Y. Mao, B. Du and Y. Zhuang, W. Tan, W. Huang, Y. Zhao, D. Liu and T. Wang, *Macromolecules*, 2020, **53**, 3747−3755.

5. L. Deng, N. Zhou, S. Tang and Y. Li, *Phys. Chem. Chem. Phys.*, 2019, **21**, 16804--16817.

6. W. Miao, Y. Feng, Q. Wu, W. Sheng, M. Li, Q. Liu, E. Hao and L. Jiao, *J. Org. Chem.*, 2019, **84**, 9693–9704.

7. Z. Feng, L. Jiao, Y. Feng, C. Yu, N. Chen, Y. Wei, X. Mu and E. Hao, *J. Org. Chem.*, 2016, **81**, 6281−6291.

8. G. Fernández, M. Stolte, V. Stepanenko and F. Würthner, *Chem. Eur. J.*, 2013, **19**, 206–217.

9. J. Gershberg, F. Fennel, T. H. Rehm, S. Lochbrunner and F. Würthner, *Chem. Sci.*, 2016, **7**, 1729–1737.

10. T. E. Kaiser, V. Stepanenko and F. Würthner, *J. Am. Chem. Soc.*, 2009, **131**, 6719–6732.

11. P. Jonkheijm, P. Schoot, A. P. H. J. Schenning and E. W. Meijer, *Science*, 2006, **313**, 80–83.

12. W. Cao and E. M. Sletten, *J. Am. Chem. Soc*., 2018, **140**, 2727-2730.

13. L. J. Patalag, L. P. Ho, P. G. Jones and D. B. Werz, *J. Am. Chem. Soc*., 2017, **139**, 15104-15113.

14. W. Liptay, R. Wortmann, H. Schaffrin, O. Burkhard, W. Reitinger and N. Detzer, *Chem. Phy.*, 1988, **120**, 429-438.

15. L. Zong, H. Zhang, Y. Li, Y. Gong, D. Li, J. Wang, Z. Wang, Y. Xie, M. Han, Q. Peng, X. Li, J. Dong, J. Qian, Q. Li and Z. Li, *ACS Nano*, 2018, **12**, 9532−9540.

16. Y. Zhang, L. Feng, J. Wang, D. Tao, C. Liang, L. Cheng, E. Hao and Z. Liu, *Small*, 2018, **14**, 1802991.

17. W. Ren, Y. Yan, L. Zeng, Z. Shi, A. Gong, P. Schaaf, D. Wang, J. Zhao, B. Zou, H. Yu, G. Chen, E. M. B. Brown and A. Wu, *Adv. Health. Mater.,* 2015, **4**, 1526-1536.

18. Y. Liu, K. Ai, J. Liu, M. Deng, Y. He and L. Lu, *Adv. Mater.*, 2013, **25**, 1353–1359.

19. D. Wang, C. Cheng, Q. Wu, J. Wang, Z. Kang, X. Guo, H. Wu, E. Hao and L. Jiao, *Org. Lett.*, 2019, **21**, 5121−5125.

20. X. Guo, H. Wu, W. Miao, Y. Wu, E. Hao and L. Jiao, *J. Porphyrins. Phthalocyanines*, 2019, **23**, 1505-1514.

21. G. Jiao, X. He, X. Li, J. Qiu, H. Xu, N. Zhang and S. Liu, *RSC Adv.*, 2015, **5**, 53240-53244.

22. Y. Cakmak, S. Kolemen, S. Duman, Y. Dede, Y. Dolen, B. Kilic, Z. Kostereli, L. T. Yildirim, A. L. Dogan, D. Guc and E. U. Akkaya, *Angew. Chem. Int. Ed.*, 2011, **50**, 11937–11941.

23. R. Liu, J. Tang, Y. Xu, Y. Zhou and Z. Dai, *Nanotheranostics*, 2017, **1**, 430-439.